IEEE Access
Multidisciplinary | Rapid Review | Open Access Journal

Received 25 March 2024, accepted 4 April 2024, date of publication 16 April 2024, date of current version 24 April 2024.

Digital Object Identifier 10.1109/ACCESS.2024.3389706

RESEARCH ARTICLE

Inkjet Printed Flexible Dual-Band Dual-Sense Circularly Polarized Patch Antenna

ABDUL RAKIB HOSSAIN, (Member, IEEE), MD. SAMIUL ISLAM SAGAR, ALEKS ALEKSANDROVICH MERTVYY, (Member, IEEE), PRAVEEN KUMAR SEKHAR, (Member, IEEE), AND TUTKU KARACOLAK, (Member, IEEE)
School of Engineering and Computer Science, Washington State University Vancouver, Vancouver, WA 98686, USA
Corresponding author: Abdul Rakib Hossain (abdul.hossain@wsu.edu)

This work was supported in part by the National Science Foundation (NSF) under Grant ECCS-2104513.

ABSTRACT This research proposes an inkjet printed dual-band dual-sense circularly polarized antenna using CPW-feeding on PET substrate. The antenna is designed and optimized using ANSYS HFSS, which operates at 4.01 GHz - 5.05 GHz (22.96%) and 6.23 GHz - 7.58 GHz (19.55%) with a return loss of < -10 dB. On top of that, the antenna shows an axial ratio of less than 3 dB at 4.23 GHz - 4.62 GHz (8.81%) and 7.11 GHz - 7.36 GHz (3.45%), whereas left hand circular polarization (LHCP) is observed in the first band and right hand circular polarization (RHCP) is observed in the second band. The overall dimensions of the antenna is 0.44λ x 0.52λ x 0.002λ, where λ is the free-space wavelength at the lowest circular polarization frequency. Measurement of the fabricated version shows good agreement with the simulated version. To the best of author's knowledge, this proposed design is the first circularly polarized antenna integrating flexibility with dual-band and dual-sensing characteristics.

INDEX TERMS PET paper, dual-band dual-sense, circular polarization, inkjet printer.

I. INTRODUCTION

With the advancement of 5G network, internet of things (IoT) devices are flourishing, creating the necessity of developing lightweight, flexible, easily integrable, portable, small size, and easily manufactured antenna systems for better connectivity with the IoT framework. Along with their uses in IoT devices and consumer electronics, flexible antennas can be used in wearable sensors, RFID tags, military applications, and wireless body area networks (WBAN) [1]. Flexible materials like polyethylene terephtalate (PET) paper, liquid crystal polymer (LCP), thin glass, polydimethylsiloxane (PDMS), textile materials (fleece fabrics, denim, cotton, polyster, felt etc.) are employed as substrates while various fabrication techniques are used to realize flexible antennas such as inkjet printing, screen printing, 3-D printing, chemical etching and flexography [2], [3], [4], [5], [6]. For inkjet printing, coplanar waveguide fed (CPW-fed) antennas are widely preferred for their simple realization. Researchers have already proposed different CPW-fed antennas on PET paper for different resonance frequencies. In [7], a CPW-fed inkjet printed antenna on PET paper is presented with ultra wide band operating at 3.04 GHZ - 10.70 GHz and 15.18 GHz - 18 GHz, maintaining an average peak gain of 3.94 dB. A CPW-fed bowtie slot wide band antenna is proposed for 2.1 GHz to 4.35 GHz on PET paper [8]. However, these antennas provide linearly polarized (LP) operation, which has disadvantages like increased multipath losses, and signal attenuation due to polarization alignment mismatch of sender and receiver antenna.

Circularly polarized (CP) antennas offer improved performance over LP antennas as they radiate two orthogonal electric field vectors with equal magnitudes and one-quarter wavelength out of phase. On that account, CP antennas are better suited for flexible and moving devices as they are prone to polarization losses. In [9], a CPW-fed circular polarized design is proposed for wearable applications for 5.8 GHz. This design used a thin Rogers substrate layer along with

The associate editor coordinating the review of this manuscript and approving it for publication was Ladislau Matekovits.

a reflector layer to reduce the loading effect on the human body. This antenna has an 18.3% axial ratio bandwidth (ARBW). Saraswat and Harish [10] have proposed another CPW-fed design on polyethylene terephthalate polyester (PETP) film based substrate that has ARBW of 13.49% from 2.35 GHz - 2.69 GHz. A U-shaped slot is cut from the patch while a portion of the ground plane from the left side is taken out to introduce asymmetry to generate circular polarization. Zu et al. [11] proposed a CP antenna using Conductive Graphene Film (CGF) for 5.8 GHz applications with low SAR. Yang et al. [12] proposed a CP antenna using flexible Panasonic R-F770 substrate and ethylene-vinyl acetate(EVA) foam as the base materials. Shorting pins are used to produce two degenerated modes to achieve CP excitation. This antenna offers an on-body S11 and AR bandwidth of 6.6% and 3.85%, respectively. All of these discussed antennas are single-band in nature.

Dual-band antennas offer more flexibility for applications being compact and cheap at the same time. In order to increase the isolation between these two bands, two orthogonal circular polarization is implemented alternatively known as dual sensing. Researchers have proposed dual-band dual-sensing antennas by techniques such as coupling non-radiative resonators with the patch [13], using parasitic elements with monopole antennas [14], and using dual coupled lines [15]. Another dual-band dual-sense design of a tilted D-shaped structure using Taconic TLY-5 substrate is proposed by Altaf and Seo [16]. This tilted D-shape is created by combining a tilted I-shape and inverted C-shape structure which is responsible for CP excitation using rotating surface current. However, all of these antennas have rigid materials as the substrate. An attempt to create a dual-band dual-sense antenna on textile materials and an artificial magnetic conductor (AMC) plane is made by Joshi et al. [17]. Nevertheless, both bands are not circularly polarized in this design.

In this paper, a dual-band dual-sense CPW-fed antenna is proposed on PET paper for CP application with an ARBW of 0.39 GHz (4.23 GHz - 4.62 GHz) for LHCP and 0.25 GHz (7.11 GHz - 7.36 GHz) for RHCP radiation. This design is an attempt to harness the advantage of dual-band dual-sense CP antenna on flexible materials which can be further extended to design for conformable and wearable applications. The antenna is optimized, and parameters such as reflection coefficient (S11), axial ratio, gain, radiation efficiency, and bending characteristics are simulated based on the finite element method (FEM). A prototype of the designed antenna is fabricated using inkjet printing technology. This manuscript contains the parametric study, fabrication mechanism, and comparison of simulated and measured values of the parameters, along with the conclusion.

II. ANTENNA DESIGN

A. DESIGN CONFIGURATION

The configuration of the proposed antenna is shown in Figure 1. The antenna is printed on one side of the

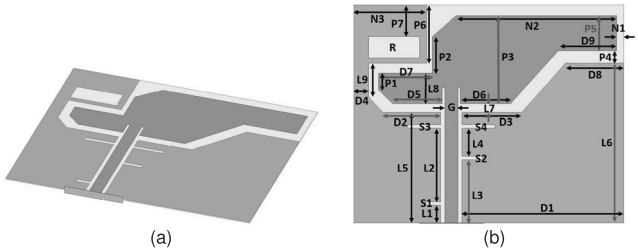

FIGURE 1. Proposed circularly polarized patch antenna. (a) Trimetric view, (b) Top view with detailed parameter marking.

TABLE 1. Optimized parameters of the proposed antenna.

Parameter	Value, mm	Parameter	Value, mm
L1	2.5	D1	22.16
L2	10.5	D2	7.9
L3	9	D3	8.16
L4	4	D4	2
L5	15.7	D5	6.82
L6	22.7	D6	6.88
L7	1.3	D7	7.37
L8	4.3	D8	8
L9	4.8	D9	8
P1	2.4	P6	8.3
P2	5.19	P7	4
P3	12.5	N1	1
P4	1.8	N2	22
P5	5	N3	10

commercially available PET paper with a dielectric constant of 3.2, a loss tangent of 0.022, and a thickness of 0.135 mm. PET paper is very light, cheap, flexible with adequate rigidity, and inkjet printer-friendly, making it useful as a substrate for low-cost and simple antenna design. The dimension of the antenna is 31 mm x 37 mm. The antenna topology is a modified ''S'' shape, which is inset-fed by a 50 Ω CPW feed line. The dimension of inset feeding is 2.2 mm x 0.35 mm. The ground plane has slots on both sides of the feed line. These slots are marked as S1 and S3 on the left side and S2 and S4 on the right side. All slots are 0.5 mm wide. The lengths of S1, S2, S3, and S4 are 2 mm, 2.8 mm, 4.5 mm, and 4.5 mm, respectively. The ground plane also has a rectangular cut in the upper left portion, which increases the ARBW slightly along with reducing the amount of ink needed to print the antenna. The dimension of the rectangular cut is 7 mm x 3 mm. The structure of the antenna is simulated and optimized by ANSYS HFSS. The optimized parameters of the antenna are given in Table 1. Please note that the substrate dimensions (31 mm x 37 mm) were not initially determined. Parametric analysis is conducted to obtain the final antenna dimensions (radiator and ground plane) and the optimized antenna is able to fit in a substrate size of 31 mm x 37 mm. The antenna design process with a detailed account of all design steps is discussed in the next section.

B. DESIGN STEPS OF THE ANTENNA

The evolution of the design is shown in Figure 2. The return loss (S11) and axial ratio of design steps are given in

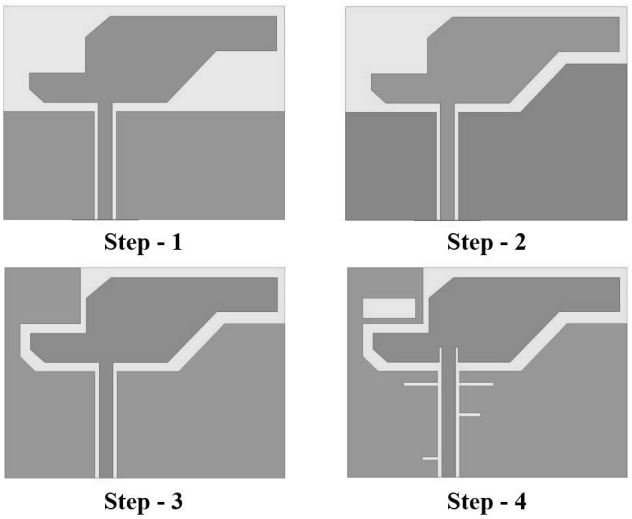

FIGURE 2. Evolution of the patch and the ground of the proposed antenna.

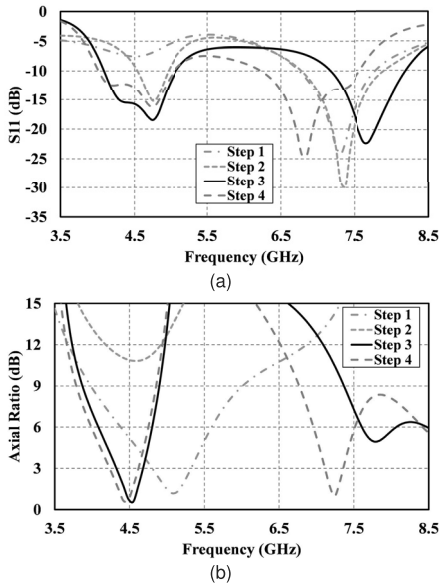

FIGURE 3. Simulated parameters for different patch design steps. (a) S11, (b) Axial ratio.

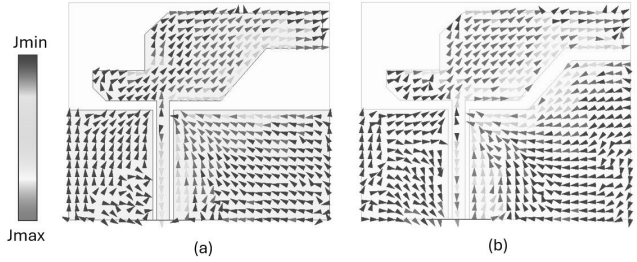

FIGURE 4. Simulated surface current distribution at 4.75 GHz. (a) Design step 1, (b) Design step 2.

Figures 3 (a) and (b), respectively. As seen in step 1, initially a CPW-fed S-shaped patch is chosen for the radiator which contributes to a compact design since it has a longer surface current path and larger electrical size compared to other shapes such as circular or rectangular. Primarily, the antenna is designed by locating the modified S-shaped patch over the feedline. The S-shape also provides an option to corner cut which is an established way of creating circular polarization. The upper-right portion of the shape is more extended outwards to create asymmetry in the design. The feed line is shifted to the left side to create space for the ground plane to cover the extended right-side portion of the patch. This design shows a bandwidth of 1.05 GHz (6.75 GHz - 7.8 GHz) and an ARBW of 0.52 GHz (4.8 GHz −5.32 GHz). However, as bandwidths are not overlapping, the antenna will not work as a CP antenna. The symmetry of the ground plane is then broken by placing a trapezium over the right side (step 2). Increasing the current path within the ground plane improves the impedance matching in the lower band and adds an additional resonant frequency around 4.75 GHz. This is also clearly observed in the surface current distribution at 4.75 GHz. Figure 4 shows the surface currents with and without trapezium over the right side of the ground plane. Surface currents are seen along the edge of the trapezium and increased current path leads to a second resonance at 4.75 GHz. This makes the antenna work on dual-band with bandwidths of 0.42 GHz (4.54 GHz - 4.96 GHz) and 1.14 GHz (6.78 GHz - 7.92 GHz). Nonetheless, no ARBW is observed in this case. To achieve circular polarization, simultaneous excitation of two orthogonal electric field components (horizontal and vertical) with equal amplitude and 90° phase difference is needed. In step 3, the ground plane is extended upwards on the left side by shielding the elongated left part of the S-shaped patch. This modification in the ground plane induces quadrature phase difference between the horizontal and vertical electric fields in the lower band and the antenna shows an overlapping ARBW of 0.36 GHz (4.32 GHz - 4.68 GHz) with the impedance bandwidth. The extension of the ground plane also increases the surface current length and improves the impedance matching at lower frequencies leading to a wider bandwidth for the first band (4.09 GHz - 5.07 GHz). The second band slightly shifts to the right side (7.17 GHz - 8.2 GHz). Finally, as shown in step 4, two slots on each side of the ground plane along the feed line are introduced along with inset feeding and a rectangular cut in the upper left corner of the ground plane. This improves the axial ratio in the higher band and an ARBW of 0.25 GHz (7.11 GHz - 7.36 GHz) is observed in the second band. The current path length increase due to the inclusion of slots and rectangular cut also shifts the higher band impedance bandwidth to left side (6.23 GHz-7.58 GHz) covering the ARBW. The lower band remains almost similar position with the bandwidth of 1.04 GHz (4.01 GHz - 5.05 GHz) along with an ARBW of 0.39 GHz (4.23 GHz - 4.62 GHz).

C. PARAMETRIC ANALYSIS

Figure 5 shows the effects of some important parameters of the proposed antenna. The proposed antenna has many design

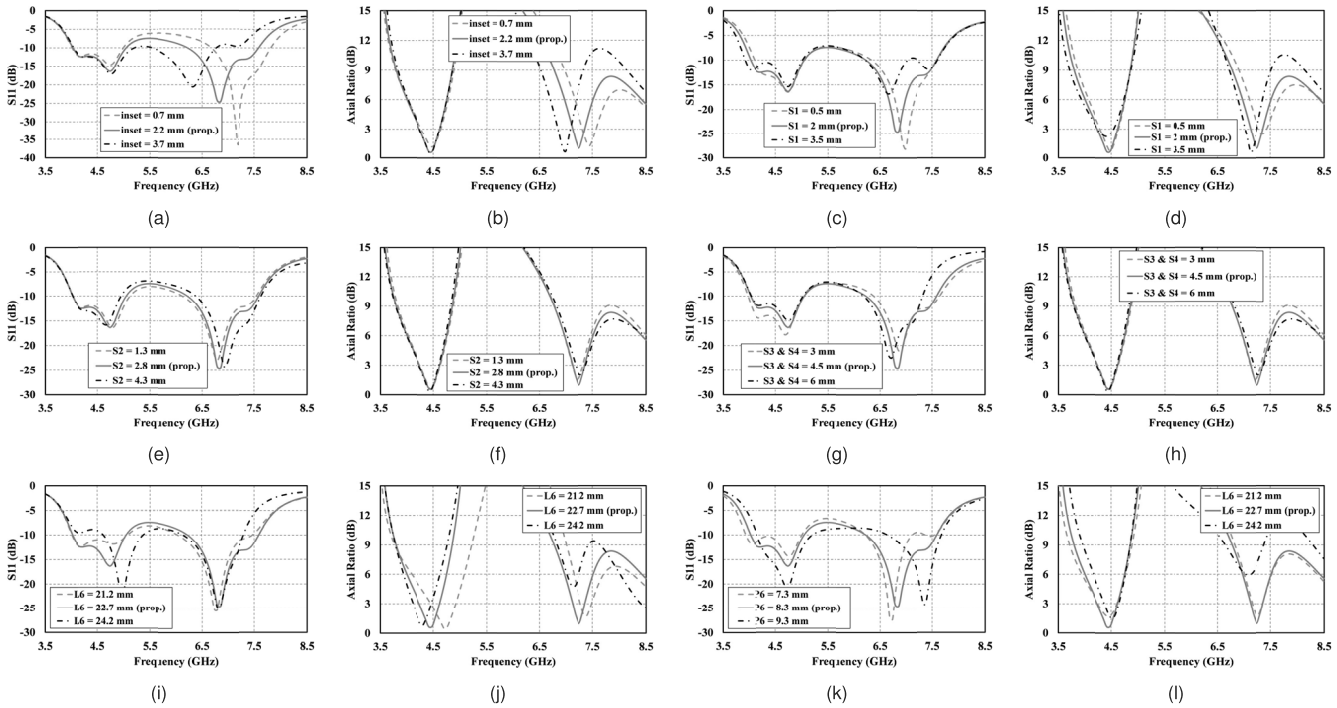

FIGURE 5. Effect of varying parameters on S11 and AR, (a) & (b) Inset gap length, (c) & (d) Length of slot S1, (e) & (f) Length of slot S2, (g) & (h) Length of slot S3 and S4, (i) & (j) Length of L6 parameter, (k) & (l) Length of P6 parameter.

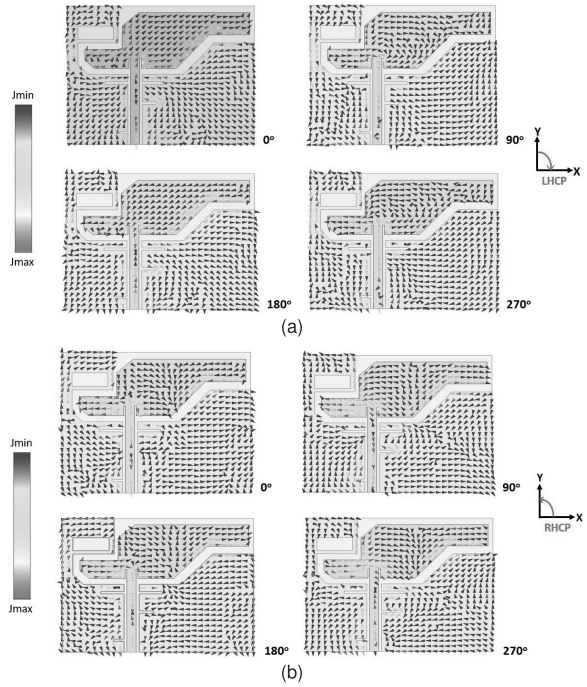

FIGURE 6. Simulated surface current distribution. (a) 4.5 GHz, (b) 7.25 GHz.

parameters that can be varied. However, the most important parameters that help to realize circular polarization are the inset gap in the patch and the slots in the ground plane (as shown in the stepwise evolution of the antenna in the previous section). Accordingly, the length of the inset gap and ground plane slots are varied to see how they affect the S11 and axial ratio of the antenna. To carry out this parametric analysis, parameters are varied with a physically realizable step size. The inset gap length is varied from 0.7 mm to 3.7 mm as our proposed length is 2.2 mm. For this parameter variation, it can be seen that the second band is shifting toward lower frequency for both S11 and axial ratio with the increase of gap length. However, the shifting distance is not the same for S11 and axial ratio which makes the second band CP realization impossible if the inset gap length keeps increasing. Immediately after, the effects of varying lengths of all four slots (S1, S2, S3, S4) by decreasing and increasing 1.5 mm from the proposed value are checked. Nonetheless, these values do not show much effect on S11 and axial ratio meaning manufacturers can have some independence while printing these gap lengths on the ground plane. The effects of L6 and P6 parameters are also considered which correspond to ground plane extensions in the bottom right and upper left sides, respectively. As seen in Figures 5 (i) and (j), if the proposed value for L6 parameter increases or decreases, impedance bandwidth and ARBW both shift, and a common frequency range where both bands work can not be obtained. A similar response is observed for P6 parameter (Figure 5 (k) and (l)).

D. CIRCULAR POLARIZATION MECHANISM, RADIATION EFFICIENCY, GAIN, AND RADIATION PATTERN ANALYSIS

To further explain the circular polarization mechanism, the surface current distribution of the proposed antenna is studied at 4.5 GHz and 7.25 GHz as shown in Figure 6.

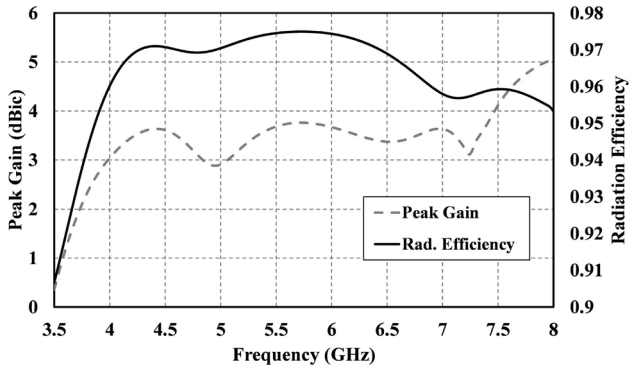

FIGURE 7. Simulated peak gain and radiation efficiency of the proposed antenna.

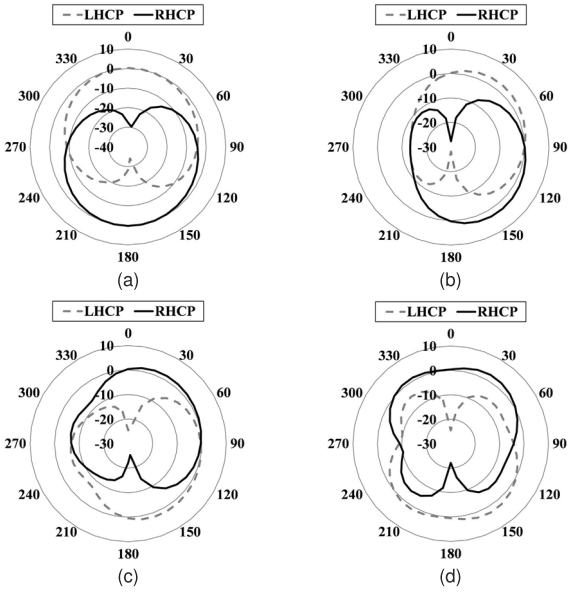

FIGURE 8. Simulated radiation pattern of LHCP and RHCP gain for frequency 4.5 GHz (a) xz plane, (b) yz plane, and for frequency 7.25 GHz (c) xz plane, (d) yz plane.

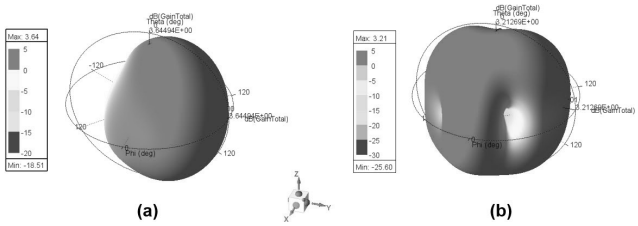

FIGURE 9. Simulated 3D radiation pattern of gain for (a) 4.5 GHz, (b) 7.25 GHz.

At 0° phase for 4.5 GHz, it is seen that the current is predominantly in +x direction along the right side of the S-shaped radiator which corresponds to the horizontal component. At 90°phase, the surface current moves towards -y direction and the dominant field components are along the extended left side of the ground plane corresponding to the vertical field component. Similarly, at 180° and 270° phases, the current is predominantly in −x and +y directions along the right side of the radiator and left side of the extended ground plane, respectively. Since the current rotates in the clockwise direction, it can be safely said that circular polarization is left-handed in the broadside direction. For 7.25 GHz, the surface current is in the +y direction at 0°phase and the dominant field components are along the slots and rectangular cut in the left side of the ground plane contributing to the vertical component. After moving the phase to 90°, the surface current direction is seen to be in −x direction along the left side of the S-shaped radiator (horizontal component). The current changes to −y and +x directions at 180° and 270° phases, respectively. As the current rotates in the anticlockwise direction, the circular polarization is right-handed with respect to the +z axis. As seen from the surface current distribution, the proposed antenna shows dual-band dual-sense characteristics. Figure 7 shows the peak gain and radiation efficiency of the antenna as a function of frequency. The average peak gain over the frequency range is around 3.35 dBic while the lowest peak gain is 2.88 dBic at 4.95 GHz and the highest peak gain is 3.63 dBic at 4.42 GHz in the first working band. In the second working band, the average peak gain is around 3.5 dBic while the lowest and highest peak gain is 3.11 dBic and 4.14 dBic respectively. The gain shows an increasing trend towards high frequency as the antenna's electrical size increases. The average radiation efficiency is over 97% in the first band while it decreases to 96% in the second band. In Figure 8, simulated far-field radiation patterns of LHCP and RHCP gain are observed in both xz (E-plane) and yz (H-plane) planes for 4.5 GHz and 7.25 GHz. At 4.5 GHz, LHCP is observed at +z direction and RHCP is observed at −z direction for both xz and yz planes. However, at 7.25 GHz, LHCP and RHCP are observed at −z and +z direction respectively for both planes. Figure 9 shows the trimetric 3D radiation pattern of gain for both 4.5 GHz and 7.25 GHz. 3D gain pattern reflects the 2D radiation pattern that is shown in Figure 8.

E. BENDING ANALYSIS

In the actual scenario, it can be possible that the antenna is used in cases where it needs to be bent as it is a flexible antenna. To demonstrate the effect of bending on antenna parameters such as return loss, axial ratio, and radiation patterns of LHCP and RHCP gain, simulations in the horizontal and vertical directions for various bending cases are performed as shown in Figure 10. Figures 11 and 12 give the effect of bending on return loss, axial ratio, and radiation pattern. As seen in Figure 11 (a) and (c), other than slight fluctuations S11 is not affected much and the reflection coefficient remains mostly stable in both bands for both horizontal and vertical bending. In terms of axial ratio, the antenna performance shows a similar response compared to the flat case in the lower band for all bending configurations. For the higher band, some differences in axial ratio bandwidth

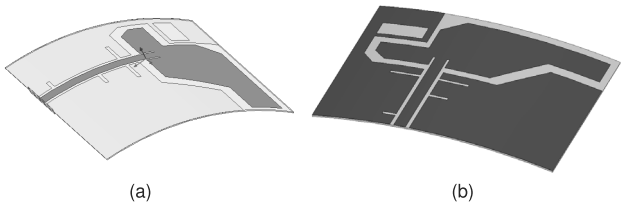

FIGURE 10. Simulated structural deformation for bending analysis (a) horizontal, (b) vertical.

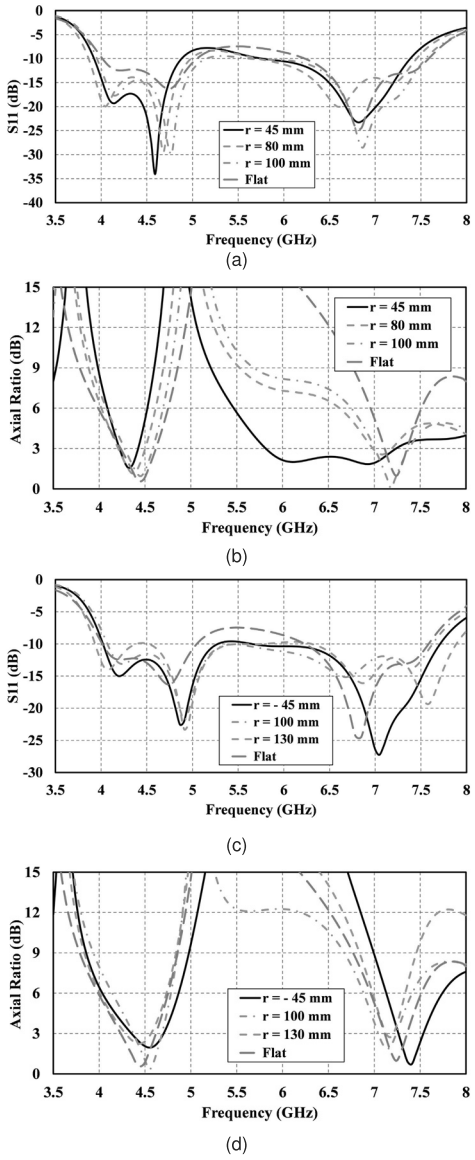

FIGURE 11. Simulated S11 parameter and axial ratio for horizontal (a) & (b) and vertical bending cases (c) & (d).

are observed in the horizontal bending case when the antenna is simulated with a very high bending configuration (r = 45 mm). Nonetheless, the axial ratio is still below 3 dB at the band of operation and maintains circular polarization. The antenna shows a similar profile with the flat case in axial ratio for other bending cases including all bending configurations

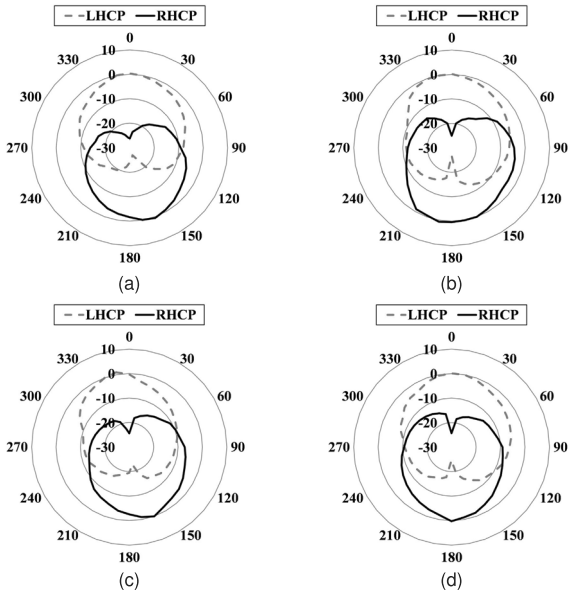

FIGURE 12. Simulated radiation pattern of LHCP and RHCP gain for frequency 4.5 GHz with horizontal bending (a) xz plane, (b) yz plane, and with vertical bending (c) xz plane, (d) yz plane.

for vertical bending. The impact of bending on antenna radiation patterns (LHCP and RHCP gain characteristics) is shown in Figure 12 at 4.5 GHz for both horizontal and vertical bending cases. As seen, bending radiation patterns show a similar pattern as the unbent case and LHCP is observed in at +z direction and RHCP is observed in −z direction for both xz and yz planes. Please note that, although not shown here similar radiation patterns between flat and bending cases are also obtained for the higher band (7.25 GHz).

III. RESULTS AND DISCUSSION

The optimized version of the antenna is printed using a Fujifilm Dimatix 2831 inkjet printer (DMP). Silver nanoparticle ink (JS-A191-S) from Novacentrix is used for printing the antenna using a Fujifilm Samba cartridge. The antenna is printed double layer to ensure high conductivity. After that, the antenna is sintered in a hotplate, gradually increasing the temperature from 90° C to 140° C. Temperature is increased in three steps with a total sintering time of 1 hour. The fabricated antenna is tested using Keysight Fieldfox N9952A microwave analyzer. Figure 13 shows the printed antenna and the measurement using a network analyzer.

Figure 14 shows the comparison of S11 and axial ratio simulation and measurement. It is noted that the simulated antenna has two resonance points at 4.22 GHz and 4.75 GHz in the first band. Measured data shows resonance points at 4.2 GHz and 4.6 GHz. However, the bandwidth matches almost exactly, starting from 4.04 GHz to 4.98 GHz. For the second band, the resonance point in the measurement shifts to 7 GHz while it is at 6.85 GHz in the simulation data. Though the resonance point shifts to the right side, the

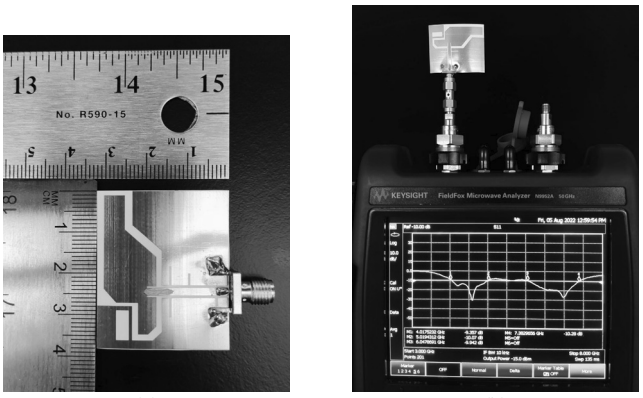

(a) (b)

FIGURE 13. (a) Fabricated antenna, (b) Antenna measurement.

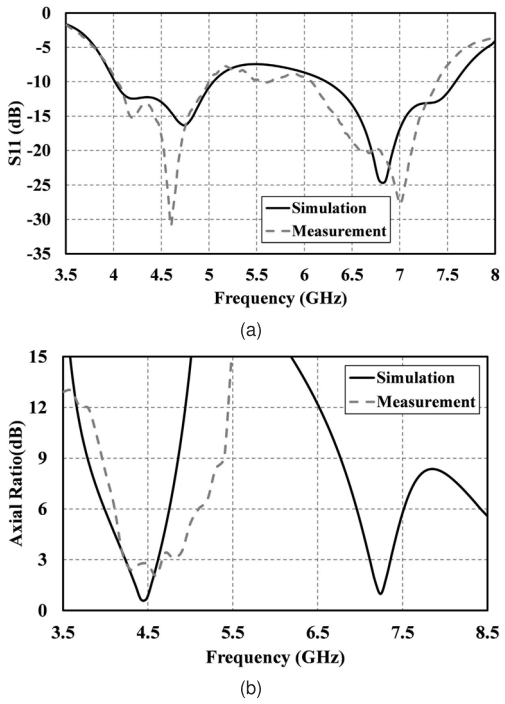

(a)

(b)

FIGURE 14. Comparison of simulated and measured (a) S11 parameter, (b) Axial ratio.

antenna band shifts to the left side, starting at 6.075 GHz and ending at 7.375 GHz. To measure the axial ratio, the antenna is placed inside an anechoic chamber and measurements are performed up to 6 GHz due to the limitations of the measurement setup. The axial ratio is under 3 dB from 4.26 GHz to 4.67 GHz. Furthermore, the radiation efficiency and peak gain are measured up to 6 GHz as shown in Figure 15. Peak gain shows an almost similar profile by varying mostly between 3 dBic and 4 dBic. Radiation efficiency varies between 0.75 to 0.9 in the measured frequency range. The reason for these minor discrepancies is inherent imperfections in printing, connector matching loss, and the effect of the measuring environment. There are some minor discrepancies between simulated and measured gain.

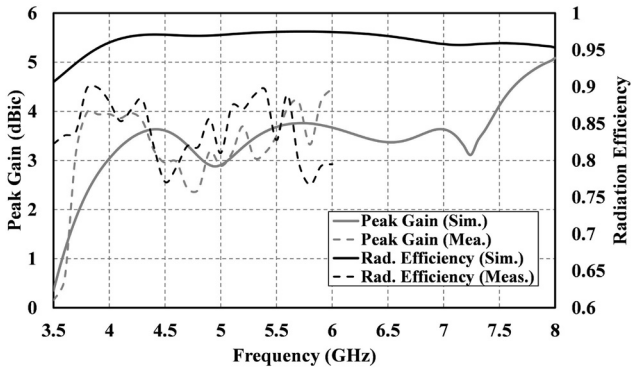

FIGURE 15. Simulated and measured peak gain and radiation efficiency of the proposed antenna.

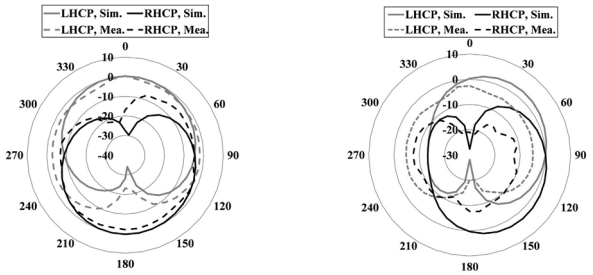

(a) (b)

FIGURE 16. Measured radiation pattern of LHCP and RHCP gain for frequency 4.5 GHz (a) xz plane, (b) yz plane.

Gain, radiation efficiency, and axial ratio are measured in an anechoic chamber whereas the S11 parameter is measured in the lab environment. Small discrepancies between simulation and measurement can be attributed to the soldering effect on the PET paper. In addition to solder roughness, losses of the SMA connector and coaxial cable may contribute to differences between the measured and simulated gain. Please note that the difference between simulated and measured gain is less than around 0.5 dBic in the circular polarization bandwidth.

Measured LHCP and RHCP radiation patterns at 4.5 GHz for both xz and yz planes are shown in Figure 16. Other than slight differences between measurements and simulations, both results confirm that LHCP is observed in at $+$z direction and RHCP is observed in $-$z direction.

As the antenna is flexible, it is necessary to check its robustness of the antenna by examining it for different bending conditions. Figure 17 demonstrates that the antenna is examined under vertical and horizontal bending conditions. For both cases, the antenna shows a similar pattern to the flat condition, which is presented in Figure 18. Thus, it can be noted that the bending conditions do not meaningfully affect the performance of the antenna.

In Table 2, the performance comparison of the proposed design with previously designed antennas is shown. As mentioned earlier, the main contribution of this work is combining dual-band dual-sense circular polarization

TABLE 2. Performance comparison of the proposed design.

Reference	Resonance Freq., GHz	%BW	% ARBW	Dimensions	Substrate	D.-band & D.-sense CP
[11]	5.8	6.9%	1.38%	0.52λ x 0.44λ x 0.019λ	Flexible	No
[12]	5.8	6.6%	3.85%	0.68λ x 0.68λ x 0.044λ	Flexible	No
[13]	2.4 & 2.68	3.3% & 2.6%	0.9% & 0.3%	1.44λ x 1.44λ x 0.024λ	Rigid	Yes
[14]	2.82	71.63%	27.45% (2.55) & 7.1% (3.53)	0.59λ x 0.71λ x 0.015λ	Rigid	Yes
[15]	2.49	7.95%	0.33% (2.4) & 0.72% (2.49)	0.44λ x 0.48λ x 0.024λ	Rigid	Yes
[17]	1.575 & 2.45	7.6% & 5.5%	10.3% & -	0.4λ x 0.4λ x 0.02λ 0.68λ x 0.68λ x 0.04λ	Flexible	Yes \No
[18]	2.1 & 3.6	1.8% & 2.6%	0.4% & 0.6%	0.49λ x 0.49λ x 0.021λ	Rigid	Yes
[19]	4.35	98.8%	4.9% (2.46) & 40.8% (5.03)	0.32λ x 0.32λ x 0.01λ	Rigid	Yes
[20]	8.75	34.29%	32.91%	0.47λ x 0.47λ x .007λ	Flexible	No
[21]	2.4	15.9%	2.72%	0.41λ x 0.41λ x 0.045λ	Flexible	No
[22]	4.3	17.53%	10.47%	0.43λ x 0.53λ x 0.002λ	Flexible	No
[23]	10.98	28.33%	11.25%	1.83λ x 1.83λ x 0.036λ	Flexible	No
[24]	2.4	14.42%	4.16%	0.24λ x 0.24λ x 0.027λ	Flexible	No
[25]	5.44	43.75%	34%	0.73λ x 0.73λ x 0.07λ	Flexible	No
[26]	5.8	25.6%	4%	0.48λ x 0.51λ	Flexible	No \Yes
Pro.	**4.53 & 6.91**	**22.96% & 19.55%**	**8.81% (4.43) & 3.45% (7.24)**	**0.44λ x 0.52λ x 0.002λ**	**Flexible**	**Yes**

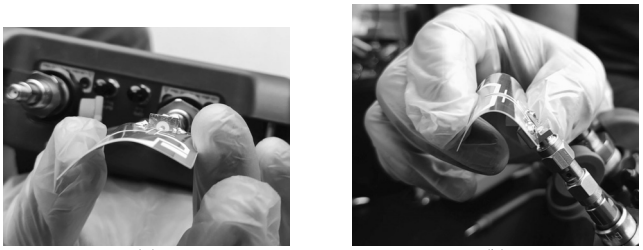

FIGURE 17. Images of fabricated antenna bending. (a) Horizontal bending, (b) Vertical bending.

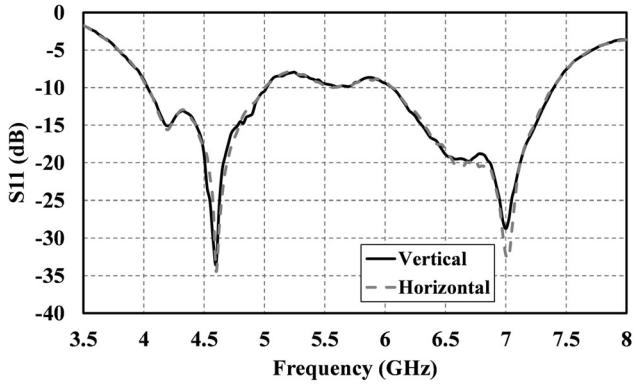

FIGURE 18. Measured S11 parameter for horizontal and vertical bending.

with flexibility. Through an extensive literature review, the authors have not found any design that meets both criteria. Therefore, the comparison is shown with some dual-band dual-sense circularly polarized antennas with rigid substrates and some single-band circularly polarized antennas with flexible substrates. As seen, the designs in [13], [15], and [18] have low impedance and axial ratio bandwidths. While [19] reports a high impedance bandwidth in a compact size, it is fabricated on a rigid substrate and is not suitable for conformal applications. Also, the antenna has a low axial ratio bandwidth in the first band. In [17], a dual-band textile antenna backed by an artificial magnetic conductor (AMC) is presented. However, this design is not circularly polarized in both bands. It has linear polarization (LP) in the higher band and circular polarization (CP) in the lower band. The design does not realize both senses of RHCP and LHCP. In addition, the antenna includes two substrate layers and an AMC plane increasing the design and fabrication complexity. Similarly, [14] has a high impedance bandwidth but it has a larger size and does not have flexibility. Furthermore, although the antenna designs of [23] and [25] are flexible and have wide axial ratio bandwidths for a single band, these designs do not have dual-band dual-sense capability, and they have a larger size compared to the proposed work. In addition, the antenna presented in [25] is based on a three-layer stripline-fed aperture-coupled structure with a high design and fabrication complexity. The design in [26] presents a flexible CPW-fed monopole-based antenna exhibiting both senses of circularly polarized rotation. Nevertheless, the design operates in a single band and has a lower axial ratio bandwidth compared to the proposed work. In addition, the study in [26] is based on only simulated data and does not present measured results to validate the theory. From Table 2, it is seen that the proposed antenna has a considerably bigger bandwidth and axial ratio with a compact size after meeting both of the design criteria.

IV. CONCLUSION

In this article, a flexible circularly polarized antenna is proposed on PET paper for dual-band dual-sense CP

application. The antenna is designed as a CPW-fed antenna with a modified ''S'' shape patch with multiple slots in the ground plane. This antenna is compact, simple, cheap, and lightweight, along with its robustness towards bending applications. Furthermore, CP antennas have higher gain and efficiency by enhancing signal reception and transmission in multipath environments making the antenna useful for moving applications like automobiles, RFID, and GPS. Specifically, this antenna can be used for FCC-allocated applications for 5G applications like 5G NR-U, Wifi [27]. By studying different antenna parameters like S11, axial ratio, gain, radiation efficiency, and radiation pattern, it can be summarized that this antenna is a great solution to consider for 4.23 GHz - 4.62 GHz and 7.11 GHz - 7.36 GHz circularly polarized applications which is the overlapping region of $S11 < -10$ dB and axial ratio (AR) < 3 dB.

ACKNOWLEDGMENT

The authors would like to thank PulseLarsen Antennas for providing the necessary setup in an anechoic chamber to measure antenna parameters.

REFERENCES

[1] S. G. Kirtania, A. W. Elger, M. R. Hasan, A. Wisniewska, K. Sekhar, T. Karacolak, and P. K. Sekhar, ''Flexible antennas: A review,'' *Micromachines*, vol. 11, no. 9, p. 847, Sep. 2020.

[2] M. R. Hasan, M. A. Riheen, P. Sekhar, and T. Karacolak, ''Compact CPW-fed circular patch flexible antenna for super-wideband applications,'' *IET Microw., Antennas Propag.*, vol. 14, no. 10, pp. 1069–1073, May 2020.

[3] H. F. Abutarboush, W. Li, and A. Shamim, ''Flexible-screen-printed antenna with enhanced bandwidth by employing defected ground structure,'' *IEEE Antennas Wireless Propag. Lett.*, vol. 19, pp. 1803–1807, 2020.

[4] S. Moscato, R. Bahr, T. Le, M. Pasian, M. Bozzi, L. Perregrini, and M. M. Tentzeris, ''Infill-dependent 3-D-printed material based on NinjaFlex filament for antenna applications,'' *IEEE Antennas Wireless Propag. Lett.*, vol. 15, pp. 1506–1509, 2016.

[5] M. E. Lajevardi and M. Kamyab, ''Ultraminiaturized metamaterial-inspired SIW textile antenna for off-body applications,'' *IEEE Antennas Wireless Propag. Lett.*, vol. 16, pp. 3155–3158, 2017.

[6] Y. Wang, Y. Huang, Y.-Z. Li, P. Cheng, S.-Y. Cheng, Q. Liang, Z.-Q. Xu, H.-J. Chen, and Z.-S. Feng, ''A facile process combined with roll-to-roll flexographic printing and electroless deposition to fabricate RFID tag antenna on paper substrates,'' *Compos. B, Eng.*, vol. 224, Nov. 2021, Art. no. 109194.

[7] S. G. Kirtania, B. A. Younes, A. R. Hossain, T. Karacolak, and P. K. Sekhar, ''CPW-fed flexible ultra-wideband antenna for IoT applications,'' *Micromachines*, vol. 12, no. 4, p. 453, Apr. 2021.

[8] M. A. Riheen, T. T. Nguyen, T. K. Saha, T. Karacolak, and P. K. Sekhar, ''CPW fed wideband bowtie slot antenna on pet substrate,'' *Prog. Electromagn. Res. C*, vol. 101, pp. 147–158, 2020.

[9] U. Ullah, I. B. Mabrouk, and S. Koziel, ''A compact circularly polarized antenna with directional pattern for wearable off-body communications,'' *IEEE Antennas Wireless Propag. Lett.*, vol. 18, pp. 2523–2527, 2019.

[10] K. Saraswat and A. R. Harish, ''Flexible dual-band dual-polarised CPW-fed monopole antenna with discrete-frequency reconfigurability,'' *IET Microw., Antennas Propag.*, vol. 13, no. 12, pp. 2053–2060, Jul. 2019.

[11] H.-R. Zu, B. Wu, Y.-H. Zhang, Y.-T. Zhao, R.-G. Song, and D.-P. He, ''Circularly polarized wearable antenna with low profile and low specific absorption rate using highly conductive graphene film,'' *IEEE Antennas Wireless Propag. Lett.*, vol. 19, pp. 2354–2358, 2020.

[12] H. C. Yang, X. Y. Liu, Y. Fan, and M. M. Tentzeris, ''Flexible circularly polarized antenna with axial ratio bandwidth enhancement for off-body communications,'' *IET Microw., Antennas Propag.*, vol. 15, no. 7, pp. 754–767, Jun. 2021.

[13] Q.-S. Wu, X. Zhang, L. Zhu, J. Wang, G. Zhang, and C.-B. Guo, ''A single-layer dual-band dual-sense circularly polarized patch antenna array with small frequency ratio,'' *IEEE Trans. Antennas Propag.*, vol. 70, no. 4, pp. 2668–2675, Apr. 2022.

[14] R. K. Saini, S. Dwari, and M. K. Mandal, ''CPW-fed dual-band dual-sense circularly polarized monopole antenna,'' *IEEE Antennas Wireless Propag. Lett.*, vol. 16, pp. 2497–2500, 2017.

[15] Z. Zhao, F. Liu, J. Ren, Y. Liu, and Y. Yin, ''Dual-sense circularly polarized antenna with a dual-coupled line,'' *IEEE Antennas Wireless Propag. Lett.*, vol. 19, pp. 1415–1419, 2020.

[16] A. Altaf and M. Seo, ''A tilted-D-shaped monopole antenna with wide dual-band dual-sense circular polarization,'' *IEEE Antennas Wireless Propag. Lett.*, vol. 17, pp. 2464–2468, 2018.

[17] R. Joshi, E. F. N. M. Hussin, P. J. Soh, M. F. Jamlos, H. Lago, A. A. Al-Hadi, and S. K. Podilchak, ''Dual-band, dual-sense textile antenna with AMC backing for localization using GPS and WBAN/WLAN,'' *IEEE Access*, vol. 8, pp. 89468–89478, 2020.

[18] Z.-X. Liang, D.-C. Yang, X.-C. Wei, and E.-P. Li, ''Dual-band dual circularly polarized microstrip antenna with two eccentric rings and an arc-shaped conducting strip,'' *IEEE Antennas Wireless Propag. Lett.*, vol. 15, pp. 834–837, 2016.

[19] H. H. Tran, T. T. Le, and T. K. Nguyen, ''Dual-band dual-sense circularly polarized antenna for S-and C-band applications,'' *Microw. Opt. Techn. Lett.*, vol. 61, no. 1, pp. 141–146, Jan. 2019.

[20] K. Fujita, K. Yoshitomi, K. Yoshida, and H. Kanaya, ''A circularly polarized planar antenna on flexible substrate for ultra-wideband high-band applications,'' *AEU-Int. J. Electron. Commun.*, vol. 69, no. 9, pp. 1381–1386, Sep. 2015.

[21] Z. H. Jiang, Z. Cui, T. Yue, Y. Zhu, and D. H. Werner, ''Compact, highly efficient, and fully flexible circularly polarized antenna enabled by silver nanowires for wireless body-area networks,'' *IEEE Trans. Biomed. Circuits Syst.*, vol. 11, no. 4, pp. 920–932, Aug. 2017.

[22] A. R. Hossain and T. Karacolak, ''CPW-fed compact circularly polarized flexible antenna for C band applications,'' in *Proc. United States Nat. Committee URSI Nat. Radio Sci. Meeting (USNC-URSI NRSM)*, Jan. 2023, pp. 246–247.

[23] H. Arun and I. Govindanarayanan, ''Circularly polarized semicircle-shaped flexible bidirectional antenna for X-band RFID applications,'' *Appl. Phys. A, Solids Surf.*, vol. 128, no. 8, pp. 1–6, Jul. 2022.

[24] A. S. M. Sayem, R. B. V. B. Simorangkir, K. P. Esselle, A. Lalbakhsh, D. R. Gawade, B. O'Flynn, and J. L. Buckley, ''Flexible and transparent circularly polarized patch antenna for reliable unobtrusive wearable wireless communications,'' *Sensors*, vol. 22, no. 3, p. 1276, Feb. 2022.

[25] Y. Chen, X. Liu, Y. Fan, and H. Yang, ''Wearable wideband circularly polarized array antenna for off-body applications,'' *IEEE Antennas Wireless Propag. Lett.*, vol. 21, pp. 1051–1055, 2022.

[26] B. F. Sadek, A. A. Abdelreheem, M. A. Abdalla, and M. E. Atrash, ''A dual-sense circularly polarized flexible asymmetric CPW-based antenna,'' in *Proc. IEEE Int. Symp. Antennas Propag. USNC-URSI Radio Sci. Meeting (USNC-URSI)*, Jul. 2023, pp. 167–168.

[27] Qualcomm. (2023). *Global 5G Spectrum Update and Innovations for Future Wireless Systems*. Accessed: Mar. 3, 2024. [Online]. Available: https://www.qualcomm.com/content/dam/qcomm-martech/dm-assets/documents/global-5g-spectrum-status-and-innovations-for-future-wireless-systems.pdf

ABDUL RAKIB HOSSAIN (Member, IEEE) received the B.Sc. degree in electrical and electronic engineering from Bangladesh University of Engineering and Technology, Dhaka, Bangladesh, in 2018. He is currently pursuing the M.Sc. degree in electrical engineering with Washington State University Vancouver, Vancouver, WA, USA. His research interests include antenna design for 5G applications, full duplex wireless technology, and RF circuit design.

MD. SAMIUL ISLAM SAGAR received the degree in electrical and electronic engineering from Khulna University of Engineering and Technology (KUET), Bangladesh, in 2019. He is currently pursuing the degree with WSUV. He has been a Teaching Assistant of electrical engineering, since Fall 2021. He is also a Researcher with the Nanomaterials-Sensor Laboratory, under the supervision of Dr. Praveen Kumar Sekhar. He had been a part of the Advanced Intelligent Multidisciplinary Systems (AIMS) Laboratory, United International University, Bangladesh, formerly, and a Research Engineer with Dr. Khondaker A. Mamun (Chairperson) with CMED Health Ltd., Bangladesh. His occupational expertise includes project management, grant writing, experiment designing, and mentoring. On the other hand, his research experience includes automation and robotics, machine learning, embedded system designing, and intelligent sensor systems. He has multiple research papers and expertise in inkjet printing technology, Ansys HFSS, and programming in Python and MATLAB.

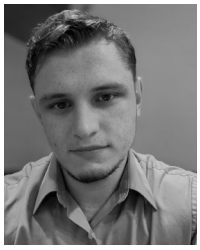

ALEKS ALEKSANDROVICH MERTVYY (Member, IEEE) received the B.Sc. degree in electrical and electronics engineering and the M.Sc. degree in electrical and electronics engineering from Washington State University Vancouver, in May 2021 and 2023, respectively, under the supervision of Dr. Tutku Karacolak. His research interests include patch antenna design, specifically focused on high-temperature substrates with MIMO system applications.

PRAVEEN KUMAR SEKHAR (Member, IEEE) received the B.E. degree (Hons.) in electrical and electronics engineering from Coimbatore Institute of Technology, in 2001, and the M.S. degree in microelectronics and the Ph.D. degree in electrical engineering from the University of South Florida, in 2005 and 2008, respectively. Then, he was a Postdoctoral Fellow with the Sensors and Electrochemical Devices Group, Los Alamos National Laboratory (LANL), Los Alamos, NM, USA, from 2009 to 2011. He started as an Assistant Professor with the School of Engineering and Computer Science, Washington State University Vancouver (WSUV), in 2011, where he is currently an Associate Professor. He was a recipient of the Alexander Von Humboldt Fellowship for experienced researchers.

TUTKU KARACOLAK (Member, IEEE) received the B.Sc. degree in electrical and electronics engineering from Bilkent University, Turkey, in 2004, and the M.Sc. and Ph.D. degrees in electrical engineering from Mississippi State University (MSU), in 2006 and 2009, respectively. From 2010 to July 2011, he was a Postdoctoral Associate of electrical engineering with MSU. In August 2011, he joined Washington State University Vancouver, where he is currently an Associate Professor. His research interests include antenna analysis and design, full-duplex systems, flexible antennas, bioelectromagnetics, and implantable antennas. He was a recipient of the 2008 IEEE Antennas and Propagation Society Graduate Scholarship and the 2009 MSU Research Assistant of the Year Award. He also serves as an Associate Editor for IEEE Access and the Guest Editor for the *Electronics* (MDPI), Special Issue on Advanced RF, Microwave, and Millimeter-Wave Circuits and Systems.